Distinction Between Active and Passive Targeting of Nanoparticles Dictate Their Overall Therapeutic Efficacy

Tristan D. Clemons,[*,†,⊥] Ruhani Singh,[†,‡,⊥] Anabel Sorolla,[§] Nutan Chaudhari,[†] Alysia Hubbard,[∥] and K. Swaminatha Iyer[†,*]

[†]School of Molecular Sciences, University of Western Australia, 35 Stirling Highway, Crawley, Western Australia Australia, 6009

[‡]CSIRO Manufacturing, New Horizons Centre, 20 Research Way, Clayton, Victoria Australia 3168

[§]Harry Perkins Institute of Medical Research, 6 Verdun Street, Nedlands, Western Australia Australia 6009

[∥]Centre for Microscopy, Characterisation and Analysis, University of Western Australia, 35 Stirling Highway, Crawley, Western Australia Australia, 6009

Supporting Information

ABSTRACT: The role of nanoparticles in cancer medicine is vast with debate still surrounding the distinction between therapeutic efficacy of actively targeted nanoparticles versus passively targeted systems for drug delivery. While it is commonly accepted that methodologies that result in homing a high concentration of drug loaded nanoparticles to the tumor is beneficial, the role of intracellular trafficking of these nanoparticles in dictating the overall therapeutic outcome remains unresolved. Herein we demonstrate that the therapeutic outcome of drug loaded nanoparticles is governed beyond simply enabling nanoparticle internalization in cells. Using two model polymeric nanoparticles, one decorated with the GE11 peptide for active targeting of the epidermal growth factor receptor (EGFR) and the other without, we demonstrate that EGFR mediated intracellular internalization results in an enhanced therapeutic effect compared to the nontargeted formulation. Our findings demonstrate that the intracellular destination of nanoparticles beyond its ability to internalize is an important parameter that has to be accounted for in the design of targeted drug delivery systems.

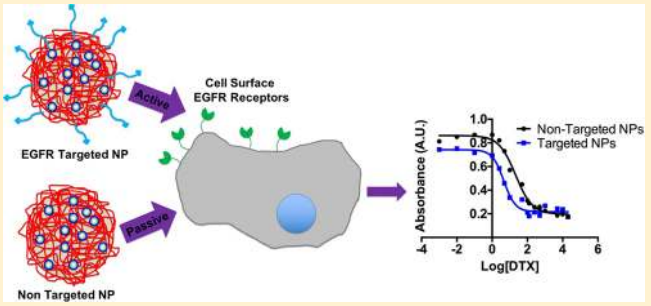

INTRODUCTION

Despite significant advances in cancer treatments and diagnosis, cancer still remains as one of the world's most devastating diseases with more than 10 million new cases reported every year.[1] Concomitant with these devastating cancer incidences are the side effects of chemotherapeutics still widely used for the treatment of this disease. Chemotherapeutics are the major class of drugs available in the arsenal against cancer, introduced in the 1950s for the treatment of these diseases.[2] However, these drugs are highly toxic and can result in severe and debilitating side effects for patients.[3,4] As a result of this, chemotherapeutics encapsulated in nanoparticle delivery vehicles are a promising field to enhance the effectiveness of these treatments in cancer while avoiding some of these side effects.[5−8] There is great interest in applying nanoparticle technology to cancer therapies largely resulting from the appealing features that nanoparticles possess. These include therapeutic protection from degradation, improved drug pharmacokinetics, improved intracellular penetration, selective tissue targeting, and the inclusion of imaging modalities.[9−11] Further to this, the increasing opportunities of "theranostic" nanoparticles which can combine both diagnostic capabilities as well as therapy within a single entity provide great promise in the fight against cancer.[12,13]

Nanoparticles due to their unique size are able to exploit the distinct cancer pathology and its molecular biology to in turn result in higher uptake and preferential targeting of therapeutics to the tumor compared to traditional treatments.[8] Broadly, this is achieved by two methods, "passive" or "active" targeting. Passive targeting is possible due to the unique changes in the cancer vasculature. Due to the rapid growth of tumors, blood vessels and junctions are not formed properly and can be loose and leaky. Owing to the unique size of nanoparticle formulations, they are able to pass through these loose junctions resulting in preferential accumulation at the tumor site over time. This phenomenon is known as the enhanced permeation and retention (EPR) effect.[10,14] As a result of this and the combinatorial advantages of nanoparticle based delivery vehicles, a number of systems have been approved by the U.S. Food and Drug Administration (FDA) for chemotherapeutic delivery. These formulations include

Received: August 29, 2018
Revised: November 1, 2018
Published: November 15, 2018

DOI: 10.1021/acs.langmuir.8b02946
Langmir XXXX, XXX, XXX−XXX

Doxil (approved 1995), a liposomal delivery system of doxorubicin, Abraxane (approved 2005), an albumin based nanoparticle delivery system of paclitaxel, and in Korea a polymeric micelle delivery vehicle of paclitaxel, Genexol-PM (approved in Korea 2007), have recently been approved.[15] All of these delivery systems are passively targeted formulations and they can suffer from a number of limitations. Lack of control in uptake in these systems can result in off target drug delivery, which may lead to multiple drug resistance, a situation where chemotherapy treatments fail in patients due to the resistance of cancer cells to one or more drugs.[10,16] Another limitation of the passive strategy is that certain tumors do not strongly exhibit the EPR effect, and the permeability of vessels can be highly heterogeneous throughout a single tumor.[16]

Active targeting of nanoparticles is where a targeting moiety (e.g., ligand, antibody, peptide) is introduced onto the nanoparticle system to target specific changes in cancer cell biology, which are highly upregulated in comparison to the healthy surrounding cells and tissues.[10,17] In this process, nanoparticles will recognize and bind to target cells through ligand−receptor interactions, and the bound nanoparticles are internalized before the drug is released inside the cell, resulting in less off target drug release compared to passively targeted systems. One method to improve the retention of nanoparticles and in turn their therapeutic payload in cancer tumors is active targeting to cell membrane receptors that are overexpressed in cancer cell lines, such as the epidermal growth factor receptor (EGFR).[18,19] EGFR up regulation has been implicated in the aggressiveness of several cancers including breast (overexpression evident in approximately 50% of triple negative breast cancer tumors),[20] renal, ovarian, colon, and nonsmall cell lung cancer.[21] As a result of this targeting, the EGF receptor is an exciting prospect for actively targeted chemotherapeutic nanoparticle formulations in the treatment of a range of cancers.

It is now widely accepted that irrespective of the targeting strategy adopted in the design for drug delivery, i.e., active or passive, it is pivotal for the nanoparticles to become therapeutically relevant, and their intracellular uptake is a crucial factor. Furthermore, it is widely established that the cellular internalization is highly dependent on the size, shape, and surface chemistry of the nanoparticles. However, what remains poorly understood is how the intracellular trafficking and intracellular destination of nanoparticles affect the overall therapeutic outcome. In this study, we show that intracellular destination of an actively targeted polymeric nanoparticle and a passively targeted nanoparticle with comparable internalization abilities differ vastly in their overall therapeutic outcome. We demonstrate this using docetaxel (DTX) loaded polymeric nanoparticles with and without GE11 peptide for targeting the EGFR, which is highly overexpressed in a number of cancers.[21]

RESULTS AND DISCUSSION

The role of nanoparticle targeting is of great interest in the application of nanoparticles for the treatment of disease and injuries, especially their role in cancer medicine. Despite this interest, there are limited studies available which look to compare actively targeted systems, such as the ERP effect, with passively targeted systems. This study demonstrates the superior effectiveness in relevant *in vitro* cancer models of an EGFR targeted polymeric nanoparticle delivery vehicle of docetaxel (DTX) to a nontargeted nanoparticle comparison. The polymeric nanoparticles were prepared by an oil-in-water emulsion process where poly(glycidyl methacrylate) (PGMA) was first synthesized and then modified with 6-maleimidohexanoic acid and rhodamine B through epoxide ring opening reactions. The attachment of the rhodamine B fluorescent probe allowed for *in vitro* fluorescent tracking of the nanoparticles, while the 6-maleimidohexanoic acid modification was used to anchor the GE11 EGFR targeting peptide to the surface of the nanoparticle. The GE11 peptide, with sequence YHWYGYTPQNVI as published previously,[22,23] was synthesized with a custom tail of four glycine units and a cysteine residue (YHWYGYTPQNVIGGGGC) to allow for consistent and precise attachment to the nanoparticle surface through thiol-maleimide chemistry. The four-glycine linkers providing flexibility in the GE11 targeting moiety away from the nanoparticle surface an important consideration for targeting peptides.[24,25] For DTX-loaded nanoparticles, the chemotherapeutic was dissolved in the "oil" phase during the emulsion process for encapsulation.

The nanoparticles are approximately 190 nm in diameter (PGMA-DTX-GE11, 195.3 nm, PDI 0.104; PGMA-DTX, 189.3 nm, PDI 0.102) with the GE11 targeted nanoparticles exhibiting a higher zeta potential (PGMA-DTX-GE11, 24.2 ± 5.8 mV; PGMA-DTX NPs, −12.6 ± 8.4 mV) (Figure 1)

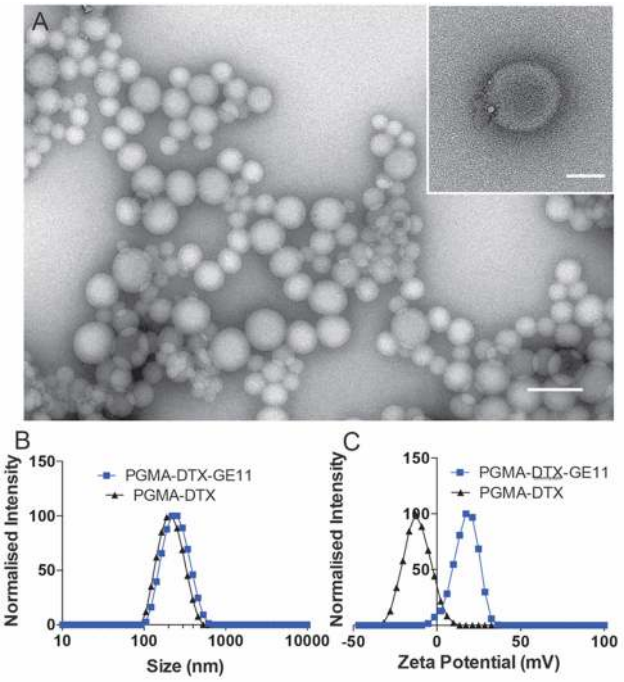

Figure 1. Physical characterization of the targeted DTX loaded nanoparticles. (A) Transmission electron microscopy images of the GE11 targeted DTX loaded nanoparticles with high magnification inset (scale 200 nm, inset 50 nm), (B) dynamic light scattering assessment of nanoparticle size, and (C) zeta potential for the targeted and nontargeted nanoparticle formulations.

resulting from the attachment of the slightly cationic peptide. Drug loading was assessed by reverse phase high-pressure liquid chromatography (HPLC) with the GE11 targeted nanoparticles found to contain 24.0 ± 1.3% w/w DTX, whereas the nontargeted nanoparticles contained a load of 21.8 ± 0.8% w/w (see the Supporting Information Figure S1 for the standard curve). The slight difference between particle loading is a result of batch-to-batch variation in the nanoparticle

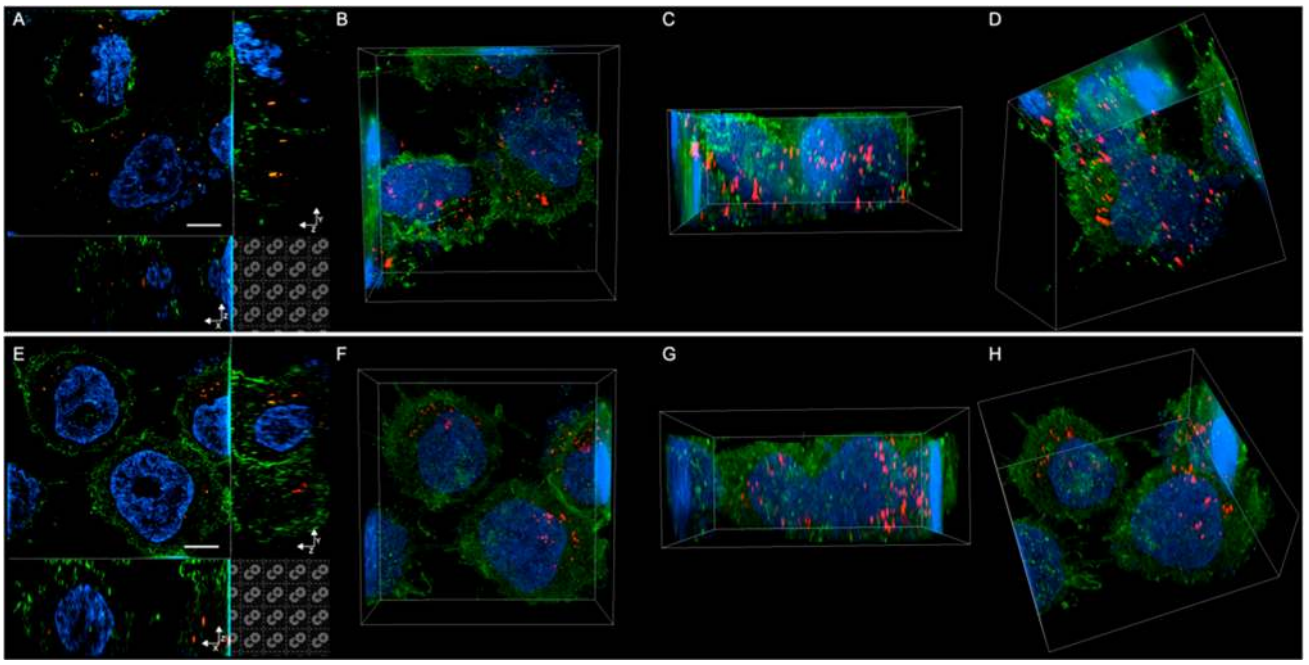

Figure 2. High-resolution confocal microscopy and structured illumination microscopy (SIM) assessment of nanoparticle internalization. (A–D) GE11-PGMA targeted nanoparticles and (E–H) PGMA nontargeted nanoparticles after 24 h incubation with MDA-MB-231 cells. (A) High-resolution confocal microscopy image taken from a central slice of the z-stack showing GE11-PGMA targeted internalization with the $x-y$, $z-y$, and $z-x$ profiles displayed. 3D reconstructions of the stack obtained from SIM images (B) top, (C) side, and (D) isometric views. (E) High-resolution confocal microscopy image taken from a central slice of the z-stack showing PGMA nontargeted internalization with the $x-y$, $z-y$, and $z-x$ profiles displayed. 3D reconstructions of the stack obtained from SIM images (F) top, (G) side, and (H) isometric views. Hoescht labeling of the nuclei (blue), anti-EGFR (green), and rhodamine labeled nanoparticles (red). Scale bars are 5 μm.

emulsion preparation process. Quantification of the maleimide functionalization and the subsequent attachment of GE11 targeting peptide was achieved using a Fluorometric Thiol Quantification Assay Kit. Attachment of GE11 peptide was found to be 22.4 nmol mg^{-1} of the targeted nanoparticle formulation (see the Supporting Information Figure S2). From physical characterization it was evident that the nanoparticles were similar in size, shape, and drug loading with the major difference being the attachment of the GE11 targeting peptide. Drug release was assessed by HPLC, and it was evident that DTX was released at a faster rate from the PGMA nontargeted nanoparticle (71.2% DTX released) when compared to the GE11 targeted nanoparticle (57.1% released) over a period of 6 days (Supporting Information Figure S3). At 24 h, the nontargeted formulation had released 7.2% more DTX then the GE11 targeted formulation, an important result with downstream *in vitro* experiments based on 24 h incubation with the therapeutic nanoparticles for comparison.

The uptake of both the GE11 targeted and the nontargeted nanoparticle without DTX loading was assessed by confocal microscopy in the breast cancer cell line MDA-MB-231. MDA-MB-231 cells were chosen as DTX has been used extensively in the treatment of breast cancers, and the overexpression of EGFR with these cells has been demonstrated previously.[26,27] It was anticipated the targeted nanoparticle would have enhanced cellular association and in turn increased uptake compared to the nontargeted formulation; however, this was not evident by confocal microscopy (see the Supporting Information Figure S4). In fact, the nontargeted nanoparticles had significant cellular association most likely due to nonspecific binding and cellular membrane association events. To further probe nanoparticle internalization, high-resolution structured illumination microscopy (SIM) was used to confirm uptake and make comparisons between the targeted and nontargeted nanoparticles (Figure 2 and Supporting Information S5 video links of SIM 3D reconstructions of the PGMA-GE11 NP and PGMA NP internalization). Cellular internalization was clearly evident for both nanoparticles by SIM microscopy, confirming both the targeted and nontargeted nanoparticles were successful at internalizing within a 24 h time period.

Further assessment of the nanoparticle fate once internalized was conducted by investigating the colocalization of nanoparticles with both endosomes and lysosomes by immunohistochemistry (see the Supporting Information Figure S6A,B). Quantitative analysis of these confocal images by comparing the Pearson's correlation coefficients (a measure to compare the colocalization) of both the GE11 targeted and the nontargeted PGMA nanoparticles with endosomes or lysosomes found significant differences in the intracellular localization of the nanoparticles following 24 h incubation (see the Supporting Information Figure S6C). Manders et al. were the first to use the Pearson correlation coefficient for fluorescent microscopy colocalization studies.[28] Briefly, the Pearson's correlation coefficient measures the pixel by pixel covariance in the signal levels of two images, with a perfect correlation of 1 and a perfectly inverse correlation of −1.[29] For this analysis, only the signal from the respective nanoparticle images with the endosome or lysosome immunohistochemistry images were compared to avoid background effects from alternate fluorescent labels present in the stacked image. This analysis showed the EGFR targeted nanoparticle associated significantly less with endosomes and lysosomes when compared to the nontargeted PGMA nanoparticle. Further to

this, both nanoparticles associated more with lysosomes compared to endosomes after 24 h of incubation (see the Supporting Information Figure S6). Hence despite similar levels of cellular internalization of the nanoparticles within MDA-MB-231 cells, it is apparent that the internal trafficking of these nanoparticles is affected by the EGFR targeting, which may also contribute to differences in the therapeutic delivery and efficacy of these nanoparticle drug delivery vehicles.

To assess the therapeutic efficacy of these DTX loaded nanoparticles, the half maximal inhibitory concentration (IC50) was determined in both MDA-MB-231 and the MCF-7 breast cancer cell lines, respectively (Figure 3). In

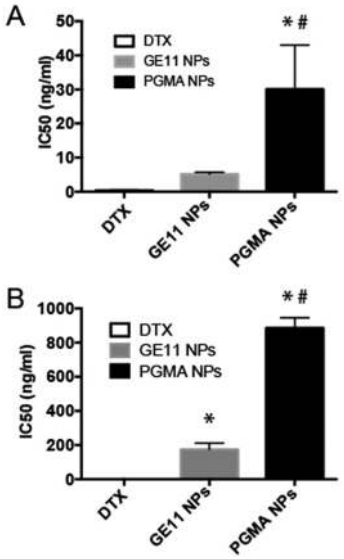

Figure 3. IC50 analysis of docetaxel (DTX), the GE11 targeted DTX nanoparticle formulation (GE11 NPs), and the untargeted PGMA DTX nanoparticles (PGMA NPs) in both MDA-MB-231 and MCF-7 cells. (A) MDA-MB-231 and (B) MCF-7 breast cancer cell lines. Data displayed as mean ± SD and statistically assessed with a one-way ANOVA followed by a Bonferroni multiple-comparisons test. Significance ($*p < 0.05$) for comparison to free DTX and ($\#p < 0.05$) for significance between the targeted GE11 NPs and the untargeted PGMA NPs.

assessing the IC50 of these formulations, it was evident that the GE11-PGMA targeted nanoparticles had a significantly lower IC50 value compared to the untargeted formulations in both MDA-MB-231 (5.1 ng/mL for GE11-PGMA NPs vs 30.1 ng/mL for PGMA NPs, Figure 3A) and MCF-7 (173.5 ng/mL for GE11-PGMA NPs vs 886.2 ng/mL for PGMA NPs, Figure 3B) cell lines. This is despite the targeted nanoparticle releasing 7% less DTX than the nontargeted nanoparticle in a 24 h period. These data presented together suggest that the active targeting of nanoparticles to cancerous cells results in active uptake and in turn direct delivery of the chemotherapeutic at the site of cell activation.

To investigate this further and to test whether the GE11-PGMA targeted nanoparticle was indeed acting through an EGFR mediated pathway, an experiment was performed to first block the EGFR receptor in culture with a blocking antibody before incubation with the targeted and untargeted DTX containing nanoparticles at their half inhibitory (IC50) concentrations, respectively (Figure 4). The presence of the EGFR blocking antibody by itself in culture media did not significantly alter cell viability (Figure 4). Pretreatment of cells

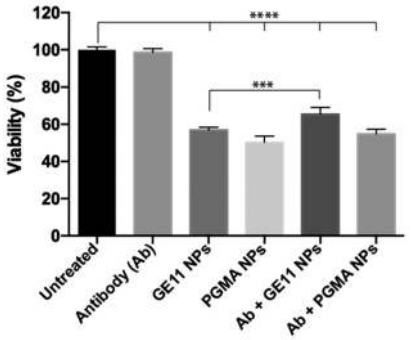

Figure 4. Blocking of the EGFR receptor significantly affects the efficacy of the GE11 targeted nanoparticle (GE11 NPs). MDA-MB-231 cells were plated and preincubated with an EGFR blocking antibody for 1 h before treatment with the IC50 concentration of each nanoparticle formulation and compared. Data displayed as mean ± SD and statistically assessed with a one-way ANOVA followed by a Bonferroni multiple-comparisons test. Significance ($***p < 0.001$, $****P < 0.0001$).

with this blocking antibody prior to nanoparticle treatment resulted in significant rescue of cell viability compared to GE11-PGMA targeted nanoparticle treatment only, but this rescue was not observed for the nontargeted PGMA nanoparticle (Figure 4). These data taken together support an active uptake of the GE11 targeted nanoparticles mediated by the EGFR due to the significant rescue observed. Furthermore, the nontargeted nanoparticles are internalized by cells via passive processes not dependent on the EGFR. Previous studies investigating similar nanoparticles found that inhibition of clathrin mediated endocytosis (chlorpromazine), caveolin mediated endocytosis (nystatin/progesterone), and micropinocytosis (*N*,*N*-dimethylamiloride) had no significant effect on PGMA based polymeric nanoparticles of similar size, and hence it was assessed that these specific cellular uptake pathways were not required for polymeric nanoparticle cellular internalization.[30] The activation of the EGFR resulting in cellular internalization via clathrin dependent uptake is also supported extensively in the literature.[31,32] It is evident that cellular uptake of a therapeutic payload into a target cell is not alone sufficient for efficacy, but the pathway of internalization plays an integral role in the therapeutic outcome of nanoparticle delivery agents.

CONCLUSIONS

Despite significant efforts, the role of active targeting moieties in nanomedicine versus passively targeted systems still remains unclear. In this study, we present data on two model polymeric drug delivery agents: one actively targeted through decoration of the nanoparticle surface with the EGFR targeting GE11 peptide; and one without, enabling passive internalization by cells. This study demonstrates the importance that active targeting of the nanoparticle system has on dictating the intracellular trafficking and furthermore the direct role that this intracellular trafficking has on the efficacy of therapeutic nanoparticles in cancer treatment. These results suggest that careful consideration of actively targeted nanoparticles cannot only influence the cellular uptake of the therapeutic cargo but also have downstream ramifications on the cellular recognition and intracellular processing of the cargo once inside the cell. For nanoparticle drug delivery systems to reach the potential they clearly possess in the treatment of cancer, thorough

studies on the efficiency of targeting need to occur to ensure optimal efficacy from these systems can be achieved.

MATERIALS AND METHODS

Materials. Glycidyl methacrylate (GMA, 97%, Sigma), 2,2′-azobis(2-methylpropionitrile) (AIBN, 0.2 M in toluene, Sigma), methyl ethyl ketone (MEK, 2-butanone; Fischer Chemical, LR grade), Pluronic F-108 (Mn = 14 600 g mol^{-1}, Sigma), 6-maleimidohexanoic acid (Sigma), rhodamine B (Kodak), sodium acetate (Sigma), Tris(2-carboxyethyl)phosphine hydrochloride (Sigma), and docetaxel (LC Laboratories, 97%) were all used as received. The GE11 peptide was synthesized with a GGGC linker sequence at the carboxyl terminus with the following sequence (YHWYGYTPQNVIGGGGC, China Peptides) and it was used as received. Tissue culture and immunohistochemistry reagents such as minimum essential medium (Invitrogen), fetal bovine serum (Invitrogen), Trypsin/EDTA (Sigma), GlutaMAX (Invitrogen), paraformaldehyde (Sigma), mouse anti-EGFR Monoclonal antibody (H11, Life Technologies, catalog no. MA5-13070), Hoechst (Sigma), goat antimouse Alexa Fluor 488 (Life Technologies, catalog no. A11001), EEA1 antibody (Abcam, ab2900), LAMP2 antibody (Santa Cruz, sc-18822 (H4B4)), goat antirabbit AF488 (ThermoFisher, A-11034), goat antimouse AF647 (ThermoFisher, A-21235), and fluorobrite (Invitrogen) were used as received. Coverglass used for SIM imaging were 170 ± 5 μm from Marienfeld, Germany. All other reagents were of analytical grade.

Poly(glycidyl methacrylate) (PGMA) Synthesis. PGMA (Mn = 186 200 g/mol, PDI 1.644) was synthesized by the free radical polymerization of glycidyl methacrylate in methyl ethyl ketone (1:1 ratio) at 80 °C for 18 h. The obtained polymer was purified by multiple precipitations from the MEK solution using methanol. Azobis(isobutyronitrile) (AIBN) was used as the initiator with product and molecular weight confirmed by NMR and GPC, respectively.

Synthesis of PGMA Nanoparticles. PGMA (200 mg) was reacted with 6-maleimidohexanoic acid (MHA, 300 mg) in MEK (30 mL, 70 °C, 5 h). The solvent was removed by a rotovap to approximately 2 mL, and the MHA modified PGMA (PGMA-MHA) precipitated in diethyl ether. The MHA-PGMA was reacted with rhodamine B (RhB, 20 mg) in MEK (30 mL, 70 °C, 5 h). The PGMA-RhB-MHA was collected by precipitating in diethyl ether and dried under a flow of N_2 to remove residual ether.

PGMA nanoparticles were prepared using a nonspontaneous emulsification process as described previously.[30,33] The modified polymer (PGMA-RhB-MHA for GE11 attachment post nanoparticle formulation or PGMA-RhB for nontargeted nanoparticles without GE11 modification, approximately 100 mg) was dissolved in a mixture of chloroform (1.5 mL) and MEK (4.5 mL) along with docetaxel (20 mg). This organic phase was added dropwise, with rapid stirring, to an aqueous phase of Pluronic F-108 (12.5 mg mL^{-1}, 30 mL), and the emulsion was homogenized with a probe-type ultrasonicator on low power for 1 min. The organics were evaporated, and the sample centrifuged at 3000*g* (45 min) to remove large aggregates and excess polymer. The supernatants were collected, and the nanoparticles centrifuged at 20 000*g* (20 min) to collect the nanoparticles. Nanoparticles were washed a further 3 times with aqueous pluronic F-108 (12.5 mg mL^{-1}, 30 mL), before storage at 4 °C of the stock and aliquots collected and freeze-dried for concentration determination.

GE11 Peptide Attachment. The GE 11 peptide was dissolved in a degassed sodium acetate buffer (50 mM, pH 4.5) prepared in Pluronic F108 (12.5 mg mL^{-1}) to a final GE11 concentration of 5 mg mL^{-1}. 6-Maleimidohexanoic acid coated nanoparticles (4 mg) were centrifuged (16 000*g*, 0.5 h) and suspended in the acetate buffer (50 mM, 1 mL). This process was repeated a second time (solution A). Tris(2-carboxyethyl)phosphine hydrochloride (TCEP, 40 mg) was dissolved in the acetate buffer (50 mM, 920 μL), and an aliquot of the GE11 peptide stock was added (80 μL) and left to incubate (0.5 h) at room temperature (RT, solution B). Solution A was combined with solution B and left to stir slowly (24 h, RT, under argon). Following peptide attachment, the nanoparticles were washed by repeated centrifugation (2× acetate buffer, final wash Pluronic F108 solution, 16 000*g*, 0.5 h) before suspending in 1× phosphate buffered saline (PBS) for ongoing *in vitro* studies.

Nanoparticle Characterization. Dilute samples of nanoparticles in MQ water were assessed for hydrodynamic size and zeta potential by dynamic light scattering on a Zetasizer Nano ZS (Malvern Instruments). Nanoparticles were drop-casted on carbon coated transmission electron microscopy (TEM) grids and imaged with an accelerating voltage of 120 kV on a JEOL 2100 TEM for physical characterization. Lyophilized aliquots of the nanoparticles were used for drug loading determination by reverse phase high-pressure liquid chromatography (RP-HPLC). The lyophilized aliquots were weighed before being suspended in methanol (1 mL). The suspension was sonicated and vortexed to dissolve the encapsulated docetaxel. The nanoparticles were removed via centrifugation (16 000*g*, 0.5 h), and the supernatant containing the dissolved free drug was analyzed using RP-HPLC. The measurements were performed on a Waters 2695 separation module with a Waters 2489 UV/vis detector (determination λ = 232 nm) using reverse phase isocratic elution (methanol−water, 70:30; flow rate at 1.0 mL min^{-1}) through a C18 column (150 mm × 4.60 mm, 5 μm, 25 ± 5 °C). The measurements were compared against a standard curve performed in identical run conditions (see the Supporting Information Figure S1 for standard curve). 6-Maleimidohexanoic acid and the final peptide concentration attached to the nanoparticles was quantified using a fluorometric thiol quantification assay kit as per the manufacturer's instructions (abcam, ab112158, see the Supporting Information Figure S2 for the standard curve).

Drug Release Experiment. Docetaxel release was assessed by RP-HPLC following a previously published protocol by Singh et al. using the above-mentioned running conditions for drug loading characterization.[34]

Cell Culture. MDA-MB-231 or MCF-7 cells were cultured in Minimum Essential Medium α with 10% fetal bovine serum (FBS), 1× GlutaMAX, and 0.15% sodium bicarbonate in a humidified incubator at 37 °C and 5% CO_2. Cells were cultured without antibiotics or antimycotics. Cells were washed with PBS, trypsinised, collected by centrifuge (1 000*g*, 5 min), and subcultured before reaching 80% confluence. Passage numbers were kept low for all experiments.

IC50 Analysis. Cells were plated in 96 well plates at 5000 cells/well in 50 μL of media. Plates were incubated for 24 h and checked visually for consistent cell density before treatments were applied. Nanoparticle concentrations were calculated by diluting according to total DTX mass from HPLC loading analysis. DTX and nanoparticle stock solutions were prepared in a minimum of 7 concentrations between 10 and 0.0001 mg/mL in DMSO. The stocks were sterilized with ultraviolet light, then diluted 1 in 250 parts media. Treatments in media were applied in triplicate at 50 μL per well then thoroughly agitated. Treatments containing DMSO were diluted by 1/2 by addition to media in wells, for a total of 0.2% v/v DMSO in 100 μL of media per well. The outer wells of each plate were filled with PBS to maintain even evaporation in treated cells. Each plate also contained three wells of cells with 100 μL of media and three with 100 μL of media + 0.2% v/v DMSO as controls. Treatments were allowed to incubate with cells for a total of 24 h at which point cell culture media containing each of the treatments were removed by inverting the plate, gently shaking, and dabbing onto a sterile paper towel. Cells were then immediately washed twice with PBS (100 μL per well), agitated for 1 min, then the PBS was removed. Warmed media was immediately applied (100 μL per well). Plates were then incubated for 48 h, accumulating to a total 72 h of *in vitro* study period.

Assays were performed using warmed CellTiter 96 AQueous One Solution Cell Proliferation Assay ((3-(4,5-dimethylthiazol-2-yl)-5-(3-carboxymethoxyphenyl)-2-(4-sulfophenyl)-2H-tetrazolium), "MTS") solution at 20 μL per well. Plates were read 3 h after the reagent was applied with a PerkinElmer EnSpire Multimode plate reader. Absorbance was measured at 490 nm in triplicate and averaged. IC50 curves were constructed from triplicate assay data in GraphPad

Prism. Data sets were normalized, then analyzed by 4-parameter nonlinear regression with an inhibition model.

EGFR Blocking Experiment. MDA-MB-231 cells were plated in 96 well plates at 5000 cells/well in 50 μL of media. After 24 h, cells were treated with a blocking antibody anti-EGFR (H11, Life Technologies, catalog no. MA5-13070) at 1 μg/mL or PBS (control) diluted in media for 1 h followed by a 24 h incubation with either targeted GE11-PGMA-DTX-NPs or untargeted PGMA-DTX-NPs at their determined IC50 concentrations with MDA-MB-231 cells. At a time 24 h after the incubation, media was changed for fresh media and the plate remained in the incubator for a further 48 h. After this time, cell viability was assessed using CellTiter-Glo 2.0 following the manufacturer's instructions.

Confocal Imaging. MDA-MB-231 cells were cultured as above on glass coverslips in 6-well plates and treated for 24 h with nanoparticle formulations (10 μg/mL), before thorough washing with PBS and fixation with 4% paraformaldehyde. Samples were immunohistochemically labeled with Mouse anti-EGFR Monoclonal antibody (1:1000, 3% BSA in PBS, 4 °C, overnight), washed with PBS (twice, 5 min), and labeled with goat antimouse Alexa Fluor 488 (1:500 in Fluorobrite, 37 °C, 30 min). Secondary was then removed, washed with PBS (twice, 5 min), and stained with Hoechst (1:1000, PBS, RT, 20 min) before washing with PBS (twice, 5 min). Colocalization studies were treated as per the above samples with the following antibodies (endosomes, 1° rabbit-EEA1, 2° antirabbit AF488 and lysosomes, 1° mouse-LAMP1, 2° antimouse AF647. Samples were mounted on glass microscope slides and imaged on a Nikon Ti-E inverted confocal microscope with a Nikon A1Si spectral detector system and a Nikon 60× oil immersion, 1.49NA objective. For super resolution imaging, images were captured on the Nikon N-SIM system with a Nikon SR 100×, 1.49NA objective. Cells were treated as above but were seeded on a coverglass of accurate thickness (170 ± 5 μm from Marienfeld, Germany) to aid in reconstruction efficiency.

Statistical Analysis. All results are displayed as means ± SD. Data was analyzed using the GraphPad Prism version 6.0 data management software to conduct ANOVA on groups of data. Statistically significant differences between each treatment were determined using Bonferroni post hoc tests (*#p < 0.05, **p < 0.01, ***p < 0.001, ****P < 0.0001).

■ ASSOCIATED CONTENT

Supporting Information

The Supporting Information is available free of charge on the ACS Publications website at DOI: 10.1021/acs.langmuir.8b02946.

Complete synthetic procedures and protocols, supporting experiments including RP-HPLC standard curve and drug loading for docetaxel, thiol assay quantification, supporting confocal imaging analysis, SIM video links, and Pearson colocalization analysis of nanoparticles with endosomes or lysosomes (PDF)

■ AUTHOR INFORMATION

ORCID

Tristan D. Clemons: 0000-0001-8042-0141

Anabel Sorolla: 0000-0001-8238-8763

K. Swaminatha Iyer: 0000-0001-9329-4930

Author Contributions

$^{\perp}$T.D.C. and R.S. contributed equally to the manuscript.

Notes

The authors declare no competing financial interest.

■ ACKNOWLEDGMENTS

The authors acknowledge the Australian Microscopy & Microanalysis Research Facility at the Centre for Microscopy, Characterization & Analysis, The University of Western Australia, funded by the University, State and Commonwealth Governments. This work was funded by the Australian Research Council (ARC), the National Health & Medical Research Council (NHMRC), and the Raine Medical Research Foundation of Australia. Tristan D. Clemons is a NHMRC Peter Doherty–Australian Biomedical Fellow. Anabel Sorolla is a recipient of a National Breast Cancer Foundation postdoctoral fellowship, and K. Swaminathan Iyer is an ARC Future fellow.

■ ABBREVIATIONS

BSA, bovine serum albumin; DTX, docetaxel; EGFR, epidermal growth factor receptor; EPR effect, enhanced permeation and retention effect; FDA, United States Food and Drug Administration; GE11, epidermal growth factor targeting peptide; GE11-PGMA-DTX-NPs, polymeric nanoparticles loaded with docetaxel and containing the GE11 targeting peptide; IC50, half maximal inhibitory concentration; PBS, phosphate buffered saline; PGMA, poly(glycidyl methacrylate); PGMA-DTX-NPs, nontargeted polymeric nanoparticles loaded with docetaxel; RP-HPLC, reverse phase high-pressure liquid chromatography; SIM, structured illumination microscopy

■ REFERENCES

(1) Stewart, B. W., Kleihues, P., Eds. *World Cancer Report 2003*; IARC Press: Lyon, France, 2003; p 351 p.

(2) DeVita, V.; Chu, E. A History of Cancer Chemotherapy. *Cancer Res.* **2008**, *68* (21), 8643–8653.

(3) Love, R. R.; Leventhal, H.; Easterling, D. V.; Nerenz, D. R. Side effects and emotional distress during cancer chemotherapy. *Cancer* **1989**, *63* (3), 604–12.

(4) Carey, M. P.; Burish, T. G. Etiology and treatment of the psychological side effects associated with cancer chemotherapy: a critical review and discussion. *Psychol. Bull.* **1988**, *104* (3), 307–25.

(5) Brannon-Peppas, L.; Blanchette, J. O. Nanoparticle and targeted systems for cancer therapy. *Adv. Drug Delivery Rev.* **2012**, *64*, 206–212.

(6) Cheng, Z. L.; Al Zaki, A.; Hui, J. Z.; Muzykantov, V. R.; Tsourkas, A. Multifunctional nanoparticles: Cost versus benefit of adding targeting and imaging capabilities. *Science* **2012**, *338* (6109), 903–910.

(7) Farokhzad, O. C.; Cheng, J. J.; Teply, B. A.; Sherifi, I.; Jon, S.; Kantoff, P. W.; Richie, J. P.; Langer, R. Targeted nanoparticle-aptamer bioconjugates for cancer chemotherapy in vivo. *Proc. Natl. Acad. Sci. U. S. A.* **2006**, *103* (16), 6315–6320.

(8) Gu, F. X.; Karnik, R.; Wang, A. Z.; Alexis, F.; Levy-Nissenbaum, E.; Hong, S.; Langer, R. S.; Farokhzad, O. C. Targeted nanoparticles for cancer therapy. *Nano Today* **2007**, *2* (3), 14–21.

(9) Shi, J. J.; Kantoff, P. W.; Wooster, R.; Farokhzad, O. C. Cancer nanomedicine: progress, challenges and opportunities. *Nat. Rev. Cancer* **2017**, *17* (1), 20–37.

(10) Peer, D.; Karp, J. M.; Hong, S.; FarokHzad, O. C.; Margalit, R.; Langer, R. Nanocarriers as an emerging platform for cancer therapy. *Nat. Nanotechnol.* **2007**, *2* (12), 751–760.

(11) Zhou, J.; Patel, T. R.; Fu, M.; Bertram, J. P.; Saltzman, W. M. Octa-functional PLGA nanoparticles for targeted and efficient siRNA delivery to tumors. *Biomaterials* **2012**, *33* (2), 583–591.

(12) Li, X.; Zhou, H. Y.; Yang, L.; Du, G. Q.; Pai-Panandiker, A. S.; Huang, X. F.; Yan, B. Enhancement of cell recognition in vitro by dual-ligand cancer targeting gold nanoparticles. *Biomaterials* **2011**, *32* (10), 2540–2545.

(13) Sawant, R. R.; Torchilin, V. P. Multifunctional nanocarriers and intracellular drug delivery. *Curr. Opin. Solid State Mater. Sci.* **2012**, *16* (6), 269−275.
(14) Matsumura, Y.; Maeda, H. A New Concept for Macromolecular Therapeutics in Cancer-Chemotherapy - Mechanism of Tumoritropic Accumulation of Proteins and the Antitumor Agent Smancs. *Cancer Res.* **1986**, *46* (12), 6387−6392.
(15) U.S. National Library of Medicine. *ClinicalTrials.gov*, https://clinicaltrials.gov/ct2/show/NCT01300533?term=BIND-014&rank=3 (accessed 2016).
(16) Jain, R. K. Barriers to Drug-Delivery in Solid Tumors. *Sci. Am.* **1994**, *271* (1), 58−65.
(17) Cho, K.; Wang, X.; Nie, S.; Chen, Z. G.; Shin, D. M. Therapeutic nanoparticles for drug delivery in cancer. *Clin. Cancer Res.* **2008**, *14* (5), 1310−6.
(18) Yang, L. L.; Mao, H.; Wang, Y. A.; Cao, Z. H.; Peng, X. H.; Wang, X. X.; Duan, H. W.; Ni, C. C.; Yuan, Q. G.; Adams, G.; Smith, M. Q.; Wood, W. C.; Gao, X. H.; Nie, S. M. Single Chain Epidermal Growth Factor Receptor Antibody Conjugated Nanoparticles for in vivo Tumor Targeting and Imaging. *Small* **2009**, *5* (2), 235−243.
(19) Sanfilippo, J. S.; Miseljic, S.; Yang, A. R.; Doering, D. L.; Shaheen, R. M.; Wittliff, J. L. Quantitative analyses of epidermal growth factor receptors, HER-2/neu oncoprotein and cathepsin D in nonmalignant and malignant uteri. *Cancer* **1996**, *77* (4), 710−716.
(20) Su, Y. C.; Burnouf, P. A.; Chuang, K. H.; Chen, B. M.; Cheng, T. L.; Roffler, S. R. Conditional internalization of PEGylated nanomedicines by PEG engagers for triple negative breast cancer therapy. *Nat. Commun.* **2017**, *8*, 15507.
(21) Herbst, R. S.; Shin, D. M. Monoclonal antibodies to target epidermal growth factor receptor-positive tumors - A new paradigm for cancer therapy. *Cancer* **2002**, *94* (5), 1593−1611.
(22) Song, S. X.; Liu, D.; Peng, J. L.; Sun, Y.; Li, Z. H.; Gu, J. R.; Xu, Y. H. Peptide ligand-mediated liposome distribution and targeting to EGFR expressing tumor in vivo. *Int. J. Pharm.* **2008**, *363* (1−2), 155−161.
(23) Li, Z.; Zhao, R.; Wu, X.; Sun, Y.; Yao, M.; Li, J.; Xu, Y.; Gu, J. Identification and characterization of a novel peptide ligand of epidermal growth factor receptor for targeted delivery of therapeutics. *FASEB J.* **2005**, *19* (14), 1978−85.
(24) Shewmake, T.; Solis, F.; Gillies, R.; Caplan, M. Effects of Linker Length and Flexibility on Multivalent Targeting. *Biomacromolecules* **2008**, *9*, 3057−3064.
(25) Liu, Y.; Cai, Y.; Liu, W.; Li, X.; Rhoades, E.; Yan, E. Triblock peptide-linker-lipid molecular design improves potency of peptide ligands targeting family B G protein-coupled receptors. *Chem. Commun.* **2015**, *51*, 6157−6160.
(26) Subik, K.; Lee, J. F.; Baxter, L.; Strzepek, T.; Costello, D.; Crowley, P.; Xing, L.; Hung, M. C.; Bonfiglio, T.; Hicks, D.; Tang, P. The Expression Patterns of ER, PR, HER2, CK5/6, EGFR, Ki-67 and AR by Immunohistochemical Analysis in Breast Cancer Cell Lines. *Breast Cancer: Basic Clin. Res.* **2010**, *4*, 35−41.
(27) Charafe-Jauffret, E.; Ginestier, C.; Monville, F.; Finetti, P.; Adelaide, J.; Cervera, N.; Fekairi, S.; Xerri, L.; Jacquemier, J.; Birnbaum, D.; Bertucci, F. Gene expression profiling of breast cell lines identifies potential new basal markers. *Oncogene* **2006**, *25*, 2273−2284.
(28) Manders, E. M. M.; Stap, J.; Brakenhoff, G. J.; Vandriel, R.; Aten, J. A. Dynamics of 3-Dimensional Replication Patterns during the S-Phase, Analyzed by Double Labeling of DNA and Confocal Microscopy. *J. Cell Sci.* **1992**, *103*, 857−862.
(29) Dunn, K. W.; Kamocka, M. M.; McDonald, J. H. A practical guide to evaluating colocalization in biological microscopy. *Am. J. Physiol-Cell Ph* **2011**, *300* (4), C723−C742.
(30) Evans, C. W.; Fitzgerald, M.; Clemons, T. D.; House, M. J.; Padman, B. S.; Shaw, J. A.; Saunders, M.; Harvey, A. R.; Zdyrko, B.; Luzinov, I.; Silva, G. A.; Dunlop, S. A.; Iyer, K. S. Multimodal analysis of PEI-mediated endocytosis of nanoparticles in neural cells. *ACS Nano* **2011**, *5* (11), 8640−8648.
(31) Kazazic, M.; Bertelsen, V.; Pedersen, K. W.; Vuong, T. T.; Grandal, M. V.; Rodland, M. S.; Traub, L. M.; Stang, E.; Madshus, I. H. Epsin 1 is Involved in Recruitment of Ubiquitinated EGF Receptors into Clathrin-Coated Pits. *Traffic* **2009**, *10* (2), 235−245.
(32) Madshus, I. H.; Stang, E. Internalization and intracellular sorting of the EGF receptor: a model for understanding the mechanisms of receptor trafficking. *J. Cell Sci.* **2009**, *122* (19), 3433−3439.
(33) Clemons, T. D.; Viola, H. M.; House, M. J.; Iyer, K. S.; Hool, L. C. Examining Efficacy of "TAT-less" Delivery of a Peptide against the L-Type Calcium Channel in Cardiac Ischemia-Reperfusion Injury. *ACS Nano* **2013**, *7* (3), 2212−2220.
(34) Singh, R.; Norret, M.; House, M. J.; Galabura, Y.; Bradshaw, M.; Ho, D. W.; Woodward, R. C.; St Pierre, T. G.; Luzinov, I.; Smith, N. M.; Lim, L. Y.; Iyer, K. S. Dose-Dependent Therapeutic Distinction between Active and Passive Targeting Revealed Using Transferrin-Coated PGMA Nanoparticles. *Small* **2016**, *12* (3), 351−359.